



# Reduced graphene oxide functionalized with a CoS<sub>2</sub>/ionic liquid composite and decorated with gold nanoparticles for voltammetric sensing of dopamine

Xuming Zhuang<sup>1</sup> · Dandan Chen<sup>1</sup> · Shuang Zhang<sup>1</sup> · Feng Luan<sup>1</sup> · Lingxin Chen<sup>1,2</sup>

Received: 28 November 2017 / Accepted: 26 January 2018 / Published online: 10 February 2018  
© Springer-Verlag GmbH Austria, part of Springer Nature 2018

## Abstract

A nanohybrid electrode was prepared by functionalizing reduced graphene oxide nanosheets (GNs) with gold nanoparticles (AuNP), CoS<sub>2</sub>, and an ionic liquid. It is shown to enable voltammetric determination of dopamine (DA). The AuNPs were electrodeposited onto the electrode that was first modified with CoS<sub>2</sub> and the IL-GNs to obtain a well-defined 3-dimensional and porous structure. The nanohybrid material displays high catalytic activity and an ultrasensitive cyclic voltammetric response to DA. The peak current (best measured at a working voltage of 0.17 V vs. Ag/AgCl) increases linearly in the 0.1 to 400 μM DA concentration range, with a 40 nM detection limit (at S/N = 3). The electrode was successfully applied to the determination of DA in spiked serum samples.

**Keywords** Electrochemical · Sensor · Nanohybrid · Dopamine · Ionic liquid · Serum samples

## Introduction

Dopamine (DA) is a neurotransmitter responsible for neuron signalling in the central nervous system of mammalian brains [1]. The concentration distribution of DA at a specific area determines the endocrine properties of the pituitary gland that is closely related to neural activity. Indeed, a modification or alteration of the DA concentration distribution may be the cause of some neurological disorders such as the Parkinson's disease or schizophrenia, respectively [2]. Therefore, it is important to develop methods able to analyze DA for the diagnosis of

neurological disorders and related medications used in nerve physiology [3]. The currently available analytical methods for the determination of DA are namely high performance liquid chromatography (HPLC) [4], UV-Vis spectroscopy [5], capillary electrophoresis [6], liquid chromatography electrospray tandem mass spectrometry [7], flow injection analysis [8], fluorescence [9], and electrochemical detection [10]. Apart from the electrochemical detection, most of the cited experimental procedures are complex, cumbersome, expensive, time consuming, and require numerous and a large amount of sample [11]. The electrochemically active DA is a catecholamine that can be directly analyzed by an electrochemical method. More specifically, DA presents an over-potential when measured on a conventional electrode and exhibits a slow electron transfer rate [12]. Consequently, exploring strategies based on the electrochemical properties of DA with electrocatalytic nanomaterials are crucial in order to develop selective and sensitive DA detection and monitoring methods.

According to reports, DA sensors prepared from metal nanomaterials, such as of silver, gold, and platinum [13], have been developed because of their suitable electrocatalytic properties. More specifically, gold nanoparticles (AuNP) have been widely used in the fabrication of sensors due to the operational simplicity of its preparation, accessible chemical modification, and good biocompatibility [14]. The

**Electronic supplementary material** The online version of this article (<https://doi.org/10.1007/s00604-018-2712-y>) contains supplementary material, which is available to authorized users.

✉ Xuming Zhuang  
xmzhuang@iccas.ac.cn

✉ Lingxin Chen  
lxchen@yic.ac.cn

<sup>1</sup> College of Chemistry and Chemical Engineering, Yantai University, Yantai 264005, China

<sup>2</sup> Key Laboratory of Coastal Environmental Processes and Ecological Remediation, Yantai Institute of Coastal Zone Research, Chinese Academy of Sciences, Yantai 264003, China

electrostatic forces between the negative holding potential on the AuNP surface and protonated dopamine in physiological pH allows significant adsorption and easy capture of the electrons from DA molecules [15], and therefore inducing the electrochemical detection of DA by the AuNP sensors. The assembling of AuNP on the electrode's surface increases the electrode conductivity and facilitates the electron transfer, improves the analytical sensitivity, selectivity, and stabilizes the sensors [16]. Moreover, AuNP exhibits superior poison resistivity toward the electro-oxidation of DA due to their large surface-to-volume ratio and the presence of highly active binding-sites on the surface of the nanoparticles.

Besides, transition-metal sulfides are regarded as a series of promising active material because they exhibit outstanding properties which are suitable for applications in energy, catalysis [17]. In particular, cobalt disulfide ( $\text{CoS}_2$ ) becomes a potential material to modify electrode because of its high catalytic ability and stability at the elevated thermal decomposition temperature [18].  $\text{CoS}_2$  coating on the surface of electrode can promote electrochemical performance of the electrode due to its superior electrochemical catalysis. Furthermore, accessible chemical modification of the surface with functional groups offers many opportunities in the development of sensors and other fields [19, 20].

Another aspect to investigate is the adsorption of the DA onto the surface of the sensors. Graphene oxide (GO) is a two-dimensional material and characterized by a layer of carbon atoms, bringing the many excellent properties of the material [21]. Indeed, GO exhibits comparable or higher electrochemical performance than carbon nanotubes and their preparation does not require separation of metal from the semiconductor or removal of catalyst and other impurities [22]. Among the functionalized GO developed for different applications, ionic liquid functionalized graphene oxide nanosheets (IL-GN) appear to exhibit adequate properties for our purpose such as strong electrical conductivity, large specific surface area and convenient dispersibility and stability [23]. Due to the positive charges, the IL-GN forms a stable composite film with negatively charged  $\text{CoS}_2$  that facilitates the adsorption and sensitive detection of DA. This is not only owe to the ionic liquids with positive charge can effectively promote the enrichment of DA, but also benefited from the network structure of IL-GN has accelerated the electron transfer.

In this paper, a DA sensor based on AuNP/ $\text{CoS}_2$ /IL-GN modified glassy carbon electrode (GCE) was fabricated to detect DA. This novel structure greatly enhances the electron transfer and electrocatalytic activity. Cyclic voltammetry (CV) was employed to evaluate the electrochemical behavior and interference resistance of the sensor. Differential pulse voltammetry (DPV) was performed to detect DA in serum.

## Experimental

### Chemicals and materials

Graphene oxide nanosheets (GNs) were purchased from Nanjing XFNano Materials Technology Company (Nanjing, China, <http://www.xfnano.com/product/pros357.aspx>). The following chemicals DA, chitosan (Chi), ascorbic acid (AA), uric acid (UA), ethylenediamine (EN), polyvinylpyrrolidone (PVP), sodium borohydride ( $\text{NaBH}_4$ ), chlorauric acid ( $\text{HAuCl}_4$ ), cobalt (II) acetate tetrahydrate, and 1-(3-aminopropyl)-3-methylimidazolium bromide (IL- $\text{NH}_2$ ) were obtained from Sigma (Shanghai, China). The potassium ferricyanides ( $\text{K}_3\text{Fe}(\text{CN})_6$  and  $\text{K}_4\text{Fe}(\text{CN})_6$ ), potassium chloride (KCl), acetic acid, and other reagents were purchased from Sinopharm Chemical Reagent Co. Ltd. (Beijing, China, <http://www.sinopharm.com>). All reagents were of analytical grade reagents and used as received. The water used in all the experiments was deionized, filtered through nanosize pores, and distilled (DDW,  $18.2 \text{ M}\Omega \text{ cm}^{-1}$ ).

### Apparatus

The experiments for CV and DPV were performed on a CHI660C electrochemical system (Chenhua Instruments, Shanghai, China) with a computer for data storage and processing. The measuring unit comprised a conventional three-electrode system, with a GCE as the working electrode, an Ag/AgCl/KCl (saturated) electrode as the reference, and a platinum wire as the counter electrode. The characterization of the different modified electrodes was determined by CV experiments in 100 mM phosphate buffer (0.1 M, pH = 7.0) or in a solution of  $\text{K}_3[\text{Fe}(\text{CN})_6]/\text{K}_4[\text{Fe}(\text{CN})_6]$  (1:1, 1 mM) containing KCl (100 mM). The DPV signals were recorded in the range of  $-0.2$  to  $0.4$  V (increment: 0.005 V; amplitude: 0.05 V; pulse width: 0.1 s; sampling width: 0.02; pulse period: 0.1 s). In all electrochemical experiments, the soaking time before measurement was 2 s.

Transmission electron microscopy (TEM, JEOL 2010F, 200 kV) was used to study the morphology and microstructure of  $\text{CoS}_2$  and nanocomposites. Scanning electron microscope (SEM) was performed on an S-4800 electron microscope (Hitachi, Ltd., Japan). All experiments were conducted at room temperature.

### Preparation procedure

The nanosheets of IL-GN were synthesized by an epoxide ring-opening reaction between GNs and IL- $\text{NH}_2$  as described in our previous report [24]. Briefly, a DDW solution (10 mL) of GNs (5 mg), IL- $\text{NH}_2$  (10 mg) and KOH (10 mg) was subjected to ultrasounds for 30 min and then heated at  $80^\circ\text{C}$  for

24 h under regular stirring. The resulting substance was centrifuged and washed with ethanol and DDW. The subsequent product was dispersed in 20 mL DDW and an aqueous solution of  $\text{NaBH}_4$  (2 M, 1 mL) was added. And the reaction mixture was heated at 80 °C for 2 h under stirring. Finally, the obtained IL-GN was washed three times with DDW.

The  $\text{CoS}_2$  nanomaterial was prepared in a closed reactor by a hydrothermal method following the steps described below [25]. EN (0.5 mL), PVP (MW = 50,000, 60 mg), and  $\text{CS}_2$  (1 mL) were successively added to an aqueous solution of cobalt (II) acetate tetrahydrate (498 mg, 2 mmol, 30 mL), which was stirred during 30 min. The resulting solution was transferred into a sealable Teflon-lined stainless steel autoclave and heated at 200 °C for 12 h. After cooling to room temperature, the subsequent powder was washed several times with DDW and then dried in vacuum at 80 °C for 12 h to finally obtain the  $\text{CoS}_2$  nanomaterial.

### Preparation of the modified electrode

The adhesives, used to provide a matrix for immobilization of nanomaterials, were prepared by heating a chitosan solution ( $1 \text{ mg mL}^{-1}$ ) at 80 °C in a water bath. The  $\text{CoS}_2$ , IL-GN, and hot solution of chitosan were mixed at the volume ratio of 1:1:0.5 and submitted to ultrasounds for 30 s. Then, a solution of the nanocomposites (5  $\mu\text{L}$ ) was deposited onto the GCE surface with a micropipette to obtain the  $\text{CoS}_2/\text{IL-GN}/\text{GCE}$  after drying naturally.

The AuNP were deposited on the surface of  $\text{CoS}_2/\text{IL-GN}/\text{GCE}$  at a constant electric potential. Briefly, the GCE modified by  $\text{CoS}_2/\text{IL-GN}$  composites was dipped into a KCl solution (100 mM) containing  $\text{HAuCl}_4$  (2 mM) at a constant electric potential of  $-0.3 \text{ V}$  for an optimal deposition duration of 300 s.

The solutions were deaerated (mainly for  $\text{O}_2$  removal) by bubbling the buffer (10 mL) and the DA standard solution (0.1 mM) with  $\text{N}_2$  gas for 5 min.

## Results and discussion

### Choice of materials

Compared with other sulfides,  $\text{CoS}_2$  is a potential material to modify electrode because of its high electrical conductivity and stability at the elevated thermal decomposition temperature.  $\text{CoS}_2$  coating on the surface of electrode can promote electrochemical performance of the electrode due to its superior electrochemical catalysis.

Graphene exhibits higher electrochemical performance than carbon nanotubes and their preparation does not require separation of metal from the semiconductor or removal of catalyst and other impurities. And GO has a large number of

polar oxygen groups, which causes both high chemical activity and hydrophilic activity between the layers of GO. Of the various ways that GO has been functionalized for different applications, ionic liquid functionalized GO (IL-GN) has particular advantages, such as strong electrical conductivity, a large specific surface area, good dispersibility, and stability.

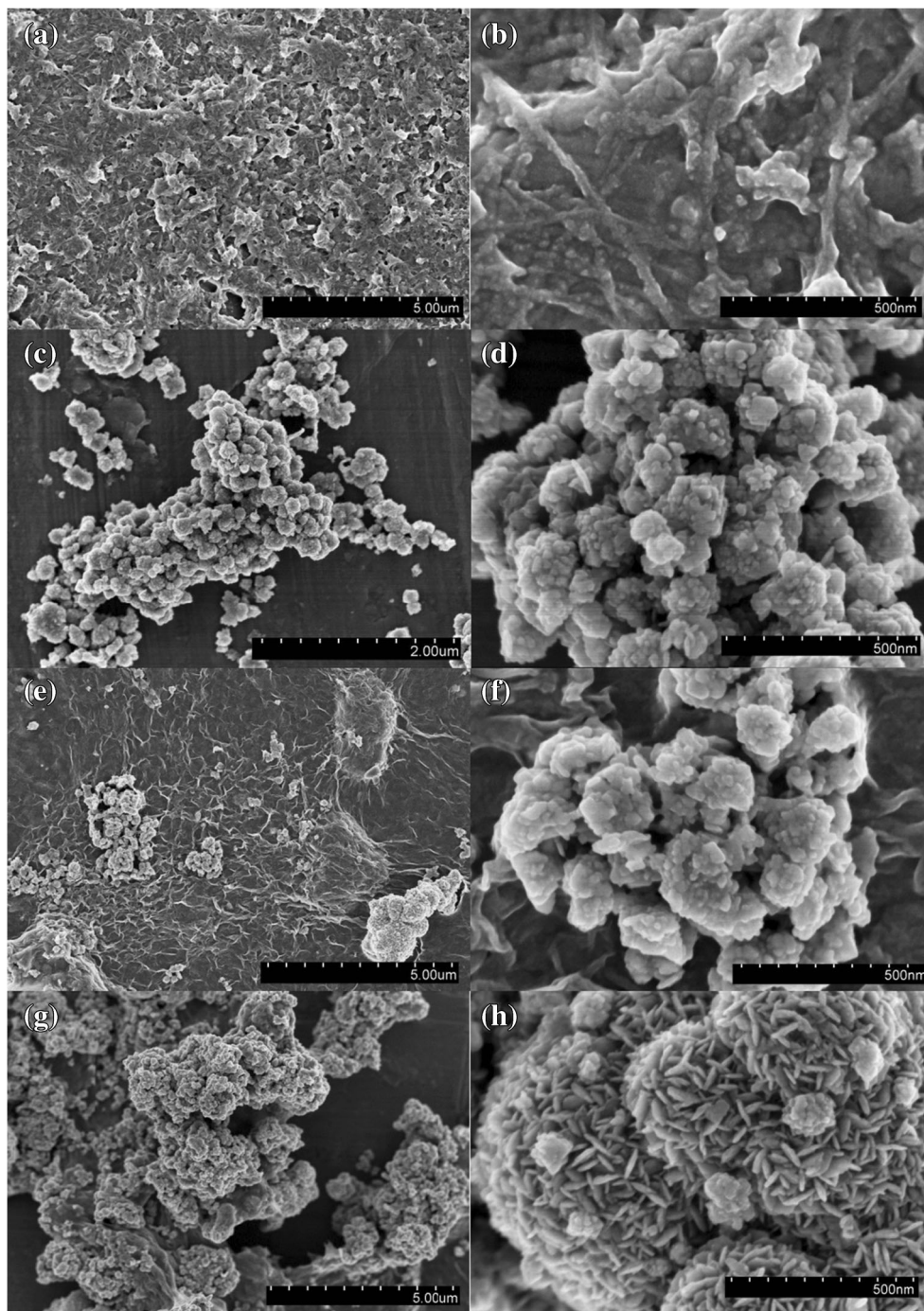
### Morphology and characterization

The TEM micrograph illustrated in Fig. S1A shows a typical thin flake-like nanocrystalline morphology of the  $\text{CoS}_2$  nanomaterials. Moreover, the more surface morphologies of the different nanomaterials were investigated using SEM. In the case of IL-GN (Fig. 1a, b), we can observe a thin layer of IL-GN displaying a typical crumpled and wrinkled structure, providing a large rough surface as scaffold for further chemical modification. The results show that the  $\text{CoS}_2$  nanomaterial (Fig. 1c, d) grew along a preferred orientation directing towards a two-dimensional nanocrystalline structure. The SEM image of a randomly chosen section of the  $\text{CoS}_2/\text{IL-GN}$  (Fig. 1e, f) nanomaterial indicates that  $\text{CoS}_2$  were uniformly fixed onto the IL-GN nanosheets surface. Moreover, the AuNP present on the surface of the IL-GN sheets exhibits a spherical structure with diameter ranging from 100 to 150 nm (Fig. 1g, h).

The powder X-ray diffraction (XRD) patterns of the synthesized  $\text{CoS}_2$  and  $\text{CoS}_2/\text{IL-GN}$  nanomaterials are represented in the Fig. 2a. The distinct diffraction peaks of both samples are attributed to the standard cubic phase of  $\text{CoS}_2$  [26]. No other obvious peaks relevant to Co or S can be further detected in the patterns.

The FT-IR spectrum of IL-GN is shown in the Fig. 2b. The bands at 2935 and 2843  $\text{cm}^{-1}$  are ascribed to the  $\text{CH}_3(\text{N})$  and  $\text{CH}_2(\text{N})$  stretching vibrations, respectively. In particular, the stretching vibration of the C-N bonds in the imidazole ring is clearly observed at 1637  $\text{cm}^{-1}$  [27], further indicating the successful synthesis of the  $\text{CoS}_2/\text{IL-GN}$  nanomaterial. Besides, the strong peak around 1060  $\text{cm}^{-1}$  is attributed to  $\text{Co}=\text{S}$  stretching in  $\text{CoS}_2$  [28]. The  $\text{CoS}_2/\text{IL-GN}$  nanomaterial is further examined using X-ray photo-electron spectroscopy (XPS) and the results are shown in the Fig. 2 and S1. The XPS spectrum of  $\text{CoS}_2/\text{IL-GN}$  (Fig. 2c) confirms the presence of the four expected elements: C, N, O, S, and Co. Moreover, the C1s spectrum shown in Fig. S1C indicates three main types of carbon bonds in the  $\text{CoS}_2/\text{IL-GN}$  nanomaterial, named C-C, C-N, and epoxy-carbon appearing at 284.6, 285.9, and 287.7 eV, respectively [29]. Interestingly, the N1 s band at 401.7 eV (Fig. 2d) presents a shoulder at a lower binding energy of 397.9 eV, which clearly confirms the presence of IL-graphene. The positions and relative intensities of the  $\text{Co}2p_{3/2}$  (Fig. S1C) and  $\text{S}2p_{3/2}$  (Fig. S2D) are correspond to the values reported in the literature [19] and confirm the presence of  $\text{CoS}_2$  in the nanomaterial.

**Fig. 1** SEM images of IL-GN (a and b), CoS<sub>2</sub> (c and d), CoS<sub>2</sub>/IL-GN (e and f), and Au/CoS<sub>2</sub>/IL-GN/GCE (g and h)

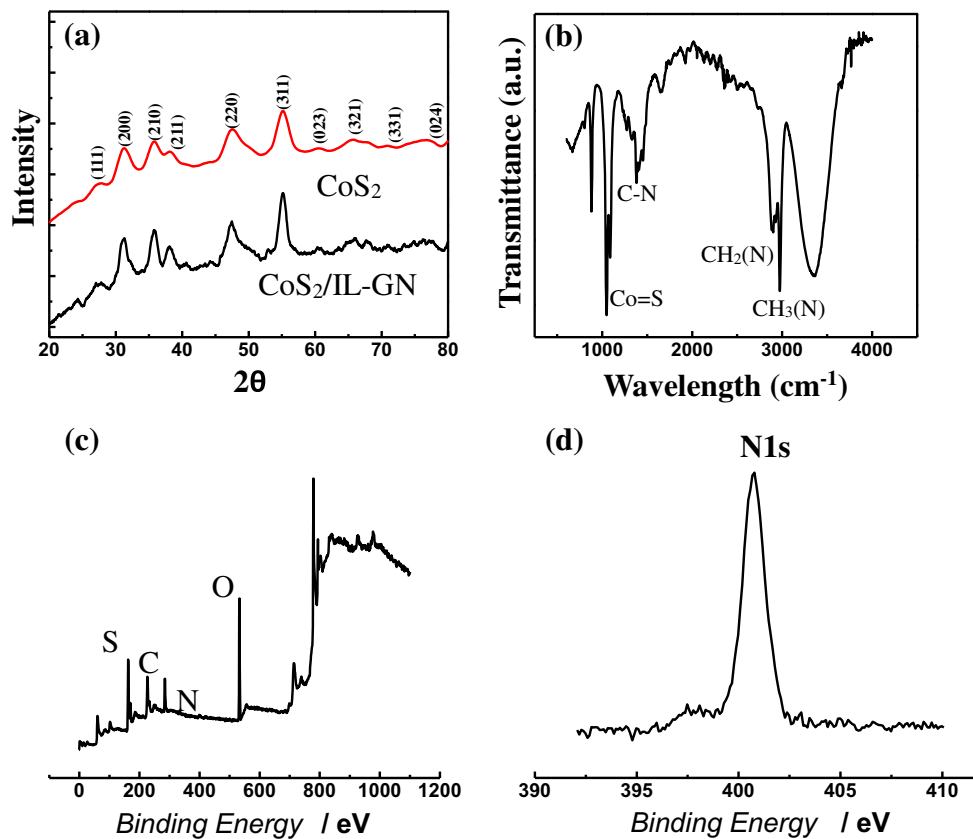


### Cyclic voltammetric behaviors of DA on the sensor

The CV behaviors of bare GCE, AuNP/GCE, CoS<sub>2</sub>/IL-GN/GCE, and AuNP/CoS<sub>2</sub>/IL-GN/GCE plunged in phosphate buffer were recorded using 0.1 mM DA. As depicted in the Fig. 3, the CV plot for the bare GCE shows an oxidation peak current at 2.629  $\mu\text{A}$  and a reduction peak at  $-1.474 \mu\text{A}$ , attributed to the lowly electron transfer between the DA solution and the electrode. As the AuNP covered the same electrode, increase of the

oxidation and reduction currents is observed by 149.7% and 273.7%, respectively. The results indicate that the oxidation and reduction currents on the CoS<sub>2</sub>/IL-GN/GCE are associated to an oxidation peak current at 3.832  $\mu\text{A}$  and a reduction peak at  $-1.158 \mu\text{A}$ , respectively. More interestingly, the oxidation and reduction currents further increase by 458.2% and 811.1% on the AuNP/CoS<sub>2</sub>/IL-GN/GCE, which indicates the highest sensitivity among these modified electrodes because the higher signal means higher sensitivity for the constant

**Fig. 2** **a** XRD pattern of CoS<sub>2</sub> (red) and CoS<sub>2</sub>/IL-GN (black). **b** FTIR spectra of CoS<sub>2</sub>/IL-GN. XPS patterns of **(c)** CoS<sub>2</sub>/IL-GN and **(d)** N1s



concentration DA. Indeed, the higher peak current of the oxidation of DA on the AuNP/CoS<sub>2</sub>/IL-GN/GCE compared to the CoS<sub>2</sub>/IL-GN/GCE, indicates a higher and synergistic electrocatalytic activity of the AuNP and CoS<sub>2</sub> towards DA [30]. Moreover, no obvious signal can be detected for the electrode modified with AuNP/CoS<sub>2</sub>/IL-GN in phosphate buffer when DA is not present (Fig.3

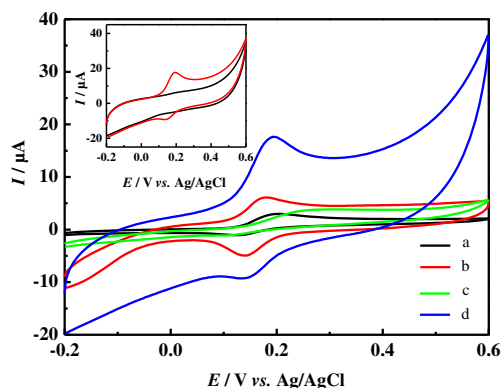


**Fig. 3** The CV curves of DA (0.1 mM) recorded on bare GCE **(a)**, Au/GCE **(b)**, CoS<sub>2</sub>/IL-GN/GCE **(c)**, and Au/CoS<sub>2</sub>/IL-GN/GCE **(d)** in phosphate buffer, scan rate set at 100 mV s<sup>-1</sup>. Inset: the CV curves of Au/CoS<sub>2</sub>/IL-GN/GCE in phosphate buffer without (black curve) and with (red curve) 0.1 mM DA, scan rate set at 100 mV s<sup>-1</sup>

insert), which highlights that no redox reaction occurs with the composite.

For further investigate the kinetic behavior, some kinetic parameter can be calculated from Laviron's Eq. [31]:

$$E_p = E^0 + \left( \frac{2.303RT}{\alpha nF} \right) \log \frac{RTk^0}{\alpha nF} + \left( \frac{2.303RT}{\alpha nF} \right) \log v \quad (1)$$

$$W_{1/2} = \frac{2.44RT}{\alpha nF} = \frac{0.0626}{\alpha n} (298K) \quad (2)$$

Where  $W_{1/2}$  is the half width of peak;  $v$  is the scan rate; and  $R$ ,  $T$  and  $F$  are molar gas constant, temperature, and Faraday's constant, respectively. Besides, according to Bard and Faulkner,  $\alpha$  can be given as:

$$\alpha = \frac{47.7}{E_p - E_{p/2}} \text{mV}(298K) \quad (3)$$

where  $E_p$  is peak potential, and  $E_{p/2}$  is the half peak potential where current is at half of the peak value. Thus,  $\alpha$  of the electrode was calculated to be 0.74, while it of CoS<sub>2</sub>/IL-GN/GCE was 0.48 and AuNP/GCE was 0.95. Moreover, the numbers of electron transferred ( $n$ ) in the electrochemical oxidation at three modified electrodes were calculated to be 1.21, 0.59 and 0.53,

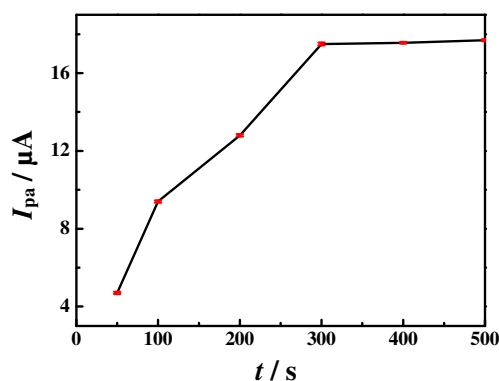


**Fig. 4** Plot of the anodic peak currents of a solution of DA (0.1 mM) in phosphate buffer) recorded at the Au/CoS<sub>2</sub>/IL-GN/GCE against the deposition duration. Scan rate set to 100 mV s<sup>-1</sup>

respectively. Obviously, the *n* value at AuNP/CoS<sub>2</sub>/IL-GN/GCE was higher than that of CoS<sub>2</sub>/IL-GN/GCE and AuNP/GCE, which affirmed that this electrode enhances the electron transfer and electrocatalytic activity due to the synergistic reaction between AuNP and CoS<sub>2</sub>.

### Effect of electrodeposition times

The electrochemical properties of the sensor fabricated at different electrodeposition durations were evaluated. To investigate the electrocatalytic activity of the obtained AuNP/CoS<sub>2</sub>/IL-GN/GCEs after depositing Au nanostructures, we conducted the electrocatalytic oxidation of DA in a 100 mM phosphate buffer containing 0.1 mM of DA and the results are shown in Fig. 4. Increasing the deposition duration enhanced the electrocatalytic activity of the electrode, which results from an extension of the electrochemical active surface area provided by the dense gold nanostructures as evidenced in previous studies [32]. However, increasing the deposition duration beyond 300 s do not significantly enhance the catalytic activity of the sense platform towards DA oxidation, implying that this maximum

**Table 1** Influences of some co-existing substances on the determination of the DA concentration fixed at 0.1 mM

Co-existing substance	Concentration (mM)	Relative error (%)
Na <sup>+</sup>	10	1.14
K <sup>+</sup>	10	1.23
Cl <sup>-</sup>	10	1.19
NO <sub>3</sub> <sup>-</sup>	10	0.87
SO <sub>4</sub> <sup>2-</sup>	10	1.17
Ca <sup>2+</sup>	5	1.76
Zn <sup>2+</sup>	5	1.68
Mg <sup>2+</sup>	5	1.57
Tartaric acid	2	2.03
Sodium acetate	2	2.31
UA	2	3.21
Lysine	2	1.56
Cysteine	2	2.35
Glucose	2	2.79

duration is the limit reached for the available electrochemically active surface area. Indeed, the nanostructures that grew at a later stage cover the active sites of the nanostructures formed at the beginning of the deposition, and the increased amount of AuNP available as the deposition duration increased (depositing after 300 s) can easily detach from the surface of the GC electrode during the CV measurement. Therefore, a value of 300 s was selected as the optimal deposition duration.

Other optimizations of experimental conditions were given in the [Electronic Supporting Material \(ESM\)](#).

### Interference on the DA detection

Furthermore, we investigated the influence of common substances co-existing with DA in samples. The electrode was tested in the presence of common interfering in-vivo substances and chemicals, such as epinephrine, 3-methoxyphenol, quercetin, vanillin, serotonin, tyramine, and dopa, in order to evaluate the implied disturbance by the co-existing substance on the result of the DA detection. When the relative error (*E<sub>r</sub>*) exceeded 5%, the tested substance is considered to be an interfering agent. The results of Table 1 show that all the tested substances do not interfere with the response of DA at the AuNP/CoS<sub>2</sub>/IL-GN/GCE. Indeed, it is found that most ions and common substances caused only negligible change even at high concentrations, i.e. Na<sup>+</sup>, K<sup>+</sup>, Cl<sup>-</sup>, NO<sub>3</sub><sup>-</sup>, SO<sub>4</sub><sup>2-</sup> (100 fold); Ca<sup>2+</sup>, Zn<sup>2+</sup>, Mg<sup>2+</sup> (50 fold); tartaric acid, sodium acetate, AA, UA, lysine, cysteine and glucose (20 fold). The results showed in Table 1 and indicate that the sensor exhibits an enhanced selectivity for the DA detection with the currently known substances. Meanwhile, the interference of AA to the DA detection was shown in the [ESM](#).

### Detection of DA in a serum sample

Under the optimal experimental conditions, the oxidation peak current (*I<sub>pa</sub>*) of DA increases as its concentration

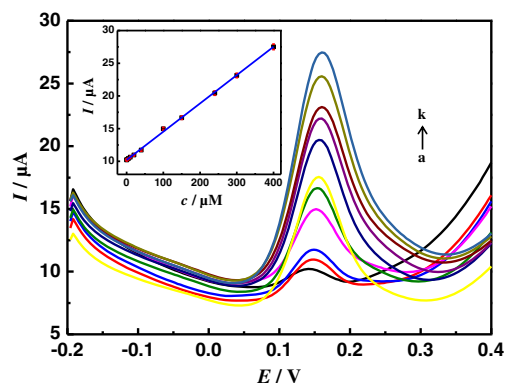


**Fig. 5** The DPV curves of DA recorded on the Au/CoS<sub>2</sub>/IL-GN/GCE in phosphate buffer (pH 7.0) with increasing concentrations of DA from 0.10 to 400.0 μM (a-k)

**Table 2** Comparison of the parameters obtained from the electrochemical detection of DA with different methods and modified electrodes

Sensors	Method	Linear range ( $\mu\text{M}$ )	Detection limit ( $\mu\text{M}$ )	References
Pd-NC <sup>a</sup> /rGO <sup>b</sup>	Amperometry	20–220	7.02	[2]
CeO <sub>2</sub> /Au	Amperometry	0.01–40	0.056	[35]
DAR <sup>c</sup>	DPV	1–12	0.1	[36]
PEDOT <sup>d</sup> /Au	DPV	0.15 - 150	0.07	[37]
MoS <sub>2</sub> /rGO	DPV	5–545	0.05	[38]
GO-MWCNT/MnO <sub>2</sub> /AuNP <sup>e</sup>	Amperometry	0.5 - 2500	0.17	[39]
pCu <sub>2</sub> O NS <sup>f</sup> -rGO	DPV	0.05–109	0.015	[40]
Au/CoS <sub>2</sub> /IL-GN/GCE	DPV	0.1–400	0.04	This study

<sup>a</sup> palladium nanocubes<sup>b</sup> reduced graphene oxide<sup>c</sup> dendritic Au rod<sup>d</sup> Poly(3,4-ethylenedioxythiophene)<sup>e</sup> gold nanoparticles<sup>f</sup> porous Cu<sub>2</sub>O nanospheres

increases from 0.1 to 400.0  $\mu\text{M}$  (Fig. 5). The DPV curve shown in Fig. 5 can be fitted by the linear regression equation  $I_{pa} (\mu\text{A}) = 0.04332c_{\text{DA}} (\mu\text{M}) + 10.2004$  ( $R^2 = 0.9983$ ) with sensitivity of  $0.6129 \mu\text{A} \cdot \mu\text{M}^{-1} \cdot \text{cm}^{-2}$ . The detection limit is  $0.04 \mu\text{M}$  ( $S/N = 3$ ), which is lower than the ones reported in previous reports [33, 34], illustrating that the modified electrode exhibits the higher sensitivity for the DA detection and a wide linear range. The Table 2 summarizes a comparison of methods, linear ranges, and detection limits obtained on Pd, Ni, and other nanomaterials used for electrochemically determination of DA in phosphate buffered solution.

### Application of the DA sensor in real samples

The utilization of the electrode for a real sample analysis was investigated by the direct detection of DA in fetal bovine serum. The determination of the DA concentration in a fetal bovine serum was estimated based on the repeated DPV responses ( $n = 5$ ) of the diluted analytes (Fig. S6). The samples were spiked with a specified concentration of DA by using the standard addition method, and we measured the DA concentration of the spiked samples. The recovery rates showing in Table S1 are all satisfying as the lowest value is 98.2% and the highest one is 102.4% within a DA concentration ranging from 0.5 to 200  $\mu\text{M}$ .

### Conclusions

We constructed a DA sensor based on AuNP/CoS<sub>2</sub>/IL-GN nanocomposites by electrodeposition. The nanocomposites were thoroughly characterized by scanning electron microscopy, spectroscopy and electrochemical methods and these results reveal unique structural features and excellent electrochemical properties. Moreover, the sensor exhibits a higher DA-detection sensitivity and more resistance against interference stemming from common co-existing substances, which

may present in real samples. The determination of the DPV curves provides satisfactory results which can be characterized by a linear response for DA concentrations ranging from 0.1 to 400.0  $\mu\text{M}$ . The DA sensor was successfully tested for the detection of trace amounts of DA in real samples. The results obtained from our study, open a new avenue for the detection of DA in real biological samples, and also present a new application of CoS<sub>2</sub> nanomaterials for electrochemical sensors. However, the clinical application of this method remains to be studied.

**Acknowledgments** This work was financially supported by the National Natural Science Foundation of China (21778047, 21675138, 21575159).

### Compliance with ethical standards

The author(s) declare that they have no competing interests.

### References

- Hammami A, Sahli R, Raouafi N (2016) Indirect amperometric sensing of dopamine using a redox-switchable naphthoquinone-terminated self-assembled monolayer on gold electrode. *Microchim Acta* 183:1137–1144
- Hsieh YS, Hong BD, Lee CL (2016) Non-enzymatic sensing of dopamine using a glassy carbon electrode modified with a nanocomposite consisting of palladium nanocubes supported on reduced graphene oxide in a nafion matrix. *Microchim Acta* 183:905–910
- Taleb M, Ivanov R, Bereznev S, Kazemi SH, Hussainova I (2017) Ultra-sensitive voltammetric simultaneous determination of dopamine, uric acid and ascorbic acid based on a graphene-coated alumina electrode. *Microchim Acta* 184:4603–4610
- Cudjoe E, Pawliszyn J (2014) Optimization of solid phase microextraction coatings for liquid chromatography mass spectrometry determination of neurotransmitters. *J Chromatogr A* 1341:1–7
- Musshoff F, Schmidt P, Dettmeyer R, Priemer F, Jachau K, Madea B (2000) Determination of dopamine and dopamine-derived (R)-/(S)-salsolinol and norsalsolinol in various human brain areas using

- solid-phase extraction and gas chromatography-mass spectrometry. *Forensic Sci Int* 113:359–366
- Qian T, Yu C, Zhou X, Ma P, Wu S, Shen LX (2014) Ultrasensitive dopamine sensor based on novel molecularly imprinted polypyrrole coated carbon nanotubes. *Biosens Bioelectron* 58:237–241
  - Schumacher F, Chakraborty S, Kleuser B, Gulbins E, Schwerdtle T, Aschner M, Bornhorst J (2015) Highly sensitive isotope-dilution liquid-chromatography-electrospray ionization-tandem-mass spectrometry approach to study the drug-mediated modulation of dopamine and serotonin levels in *Caenorhabditis elegans*. *Talanta* 144: 71–79
  - Pozo MD, Mejías J, Hernández P, Quintana C (2014) Cucurbit uril-based electrochemical sensors as detectors in flow injection analysis. Application to dopamine determination in serum samples. *Sensors Actuators B Chem* 193:62–69
  - Wu HP, Cheng TL, Tseng WL (2007) Phosphate-modified TiO<sub>2</sub> nanoparticles for selective detection of dopamine, levodopa, adrenaline, and catechol based on fluorescence quenching. *Langmuir* 23: 7880–7885
  - Numan A, Shahid MM, Omar FS, Ramesh K, Ramesh S (2017) Facile fabrication of cobalt oxide nanograin-decorated reduced graphene oxide composite as ultrasensitive platform for dopamine detection. *Sensors Actuators B Chem* 238:1043–1051
  - Li Y, Gu Y, Zheng B, Luo L, Li C, Yan X, Zhang T, Lu N, Zhang Z (2017) A novel electrochemical biomimetic sensor based on poly(Cu-AMT) with reduced graphene oxide for ultrasensitive detection of dopamine. *Talanta* 162:80–89
  - Hawley MD, Tatawawadi SV, Adams SPN (1967) Electrochemical studies of the oxidation pathways of catecholamines. *J Am Chem Soc* 89:447–450
  - Yusoff N, Pandikumar A, Ramaraj R, Ngee LH, Huang NM (2015) Gold nanoparticle based optical and electrochemical sensing of dopamine. *Microchim Acta* 182:2091–2114
  - Liu J, Xie Y, Wang K, Zeng Q, Liu R, Liu X (2017) A nanocomposite consisting of carbon nanotubes and gold nanoparticles in an amphiphilic copolymer for voltammetric determination of dopamine, paracetamol and uric acid. *Microchim Acta* 184:1739–1745
  - Zachek MK, Hermans A, Wightman RM, McCarty GS (2008) Electrochemical dopamine detection: comparing gold and carbon fiber microelectrodes using background subtracted fast scan cyclic voltammetry. *J Electroanal Chem* 614:113–120
  - Zhang MR, Chen XQ, Pan GB (2017) Electrosynthesis of gold nanoparticles/porous GaN electrode for non-enzymatic hydrogen peroxide detection. *Sensors Actuators B Chem* 240:142–147
  - Numan A, Shahid MM, Omar FS, Raffique S, Bashir S, Ramesh K, Ramesh S (2017) Binary nanocomposite based on Co<sub>3</sub>O<sub>4</sub> nanocubes and multiwalled carbon nanotubes as an ultrasensitive platform for amperometric determination of dopamine. *Microchim Acta* 184:2739–2748
  - Zhang H, Li Y, Zhang G, Wan P, Xu T, Wu X, Sun X (2014) Highly crystallized cubic cattierite CoS<sub>2</sub> for electrochemically hydrogen evolution over wide pH range from 0 to 14. *Electrochim Acta* 148:170–174
  - Faber MS, Dzedzic R, Lukowski MA, Kaiser NS, Ding Q, Jin S (2014) High-performance electrocatalysis using metallic cobalt pyrite (CoS<sub>2</sub>) micro- and nanostructures. *J Am Chem Soc* 136:10053–10061
  - Xing Z, Wang L, Yang X (2016) Cobalt disulfide nanowires as an effective fluorescent sensing platform for DNA detection. *J Mater Chem B* 4:2860–2863
  - Lu L, Guo L, Kang T, Cheng S (2017) A gold electrode modified with a three-dimensional graphene-DNA composite for sensitive voltammetric determination of dopamine. *Microchim Acta* 184: 2949–2957
  - Song H, Xue G, Zhang J, Wang G, Ye BC, Sun S, Li Y (2017) Simultaneous voltammetric determination of dopamine and uric acid using carbon-encapsulated hollow Fe<sub>3</sub>O<sub>4</sub> nanoparticles anchored to an electrode modified with nanosheets of reduced graphene oxide. *Microchim Acta* 184:843–853
  - Yang G, Zhao F, Zeng B (2014) Facile fabrication of a novel anisotropic gold nanoparticle-chitosan-ionic liquid/graphene modified electrode for the determination of theophylline and caffeine. *Talanta* 127:116–127
  - Zhuang XM, Wang HH, He T, Chen LX (2016) Enhanced voltammetric determination of dopamine using a glassy carbon electrode modified with ionic liquid-functionalized graphene and carbon dots. *Microchim Acta* 183:3177–3182
  - Kumar MK, Prataap RV, Mohan S, Jha SK (2016) Preparation of electro-reduced graphene oxide supported walnut shape nickel nanostructures, and their application to selective detection of dopamine. *Microchim Acta* 183:1759–1768
  - Qiu B, Zhao X, Xia D (2013) In situ synthesis of CoS<sub>2</sub>/RGO nanocomposites with enhanced electrode performance for lithium-ion batteries. *J Alloys Compd* 579:372–376
  - Lian J, Duan X, Ma J, Peng P, Kim T, Zheng W (2009) Hematite (α-Fe<sub>2</sub>O<sub>3</sub>) with various morphologies: ionic liquid-assisted synthesis, formation mechanism, and properties. *ACS Nano* 3:3749–3761
  - Chakraborty I, Malik PK, Moulik SP (2006) Preparation and characterisation of CoS<sub>2</sub> nanomaterial in aqueous cationic surfactant medium of cetyltrimethylammonium bromide (CTAB). *J Nanopart Res* 8:889–897
  - Guo S, Wen D, Zhai Y, Dong S, Wang E (2011) Ionic liquid-graphene hybrid nanosheets as an enhanced material for electrochemical determination of trinitrotoluene. *Biosens Bioelectron* 26: 3475–3481
  - Thanh TD, Balamurugan J, Lee SH, Kim NH, Lee JH (2016) Effective seed-assisted synthesis of gold nanoparticles anchored nitrogen-doped graphene for electrochemical detection of glucose and dopamine. *Biosens Bioelectron* 81:259–267
  - Laviron E (1979) General expression of the linear potential sweep voltammogram in the case of diffusionless electrochemical systems. *J Electroanal Chem Interfacial* 101:19–28
  - Shu H, Cao L, Chang G, He H, Zhang Y, He Y (2014) Direct electrodeposition of gold nanostructures onto glassy carbon electrodes for non-enzymatic detection of glucose. *Electrochim Acta* 132:524–532
  - Wang Y, Li Y, Tang L, Lu J, Li J (2009) Application of graphene-modified electrode for selective detection of dopamine. *Electrochem Commun* 11:889–892
  - Li SJ, He JZ, Zhang MJ, Zhang RX, Lv XL, Li SH, Pang H (2013) Electrochemical detection of dopamine using water-soluble sulfonated graphene. *Electrochim Acta* 102:58–65
  - Tong Y, Li Z, Lu X, Yang L, Sun W, Nie G, Wang Z, Wang C (2013) Electrochemical determination of dopamine based on electrosynthesized CeO<sub>2</sub>/Au composite nanofibers. *Electrochim Acta* 95: 12–17
  - Ahn M, Kim J (2012) Electrochemical behavior of dopamine and ascorbic acid at dendritic Au rod surfaces: selective detection of dopamine in the presence of high concentration of ascorbic acid. *J Electroanal Chem* 683:75–79
  - Ali A, Jamal R, Abdiryim T, Huang X (2017) Synthesis of monodispersed PEDOT/Au hollow nanospheres and its application for electrochemical determination of dopamine and uric acid. *J Electroanal Chem* 787:110–117



38. Xing L, Ma Z (2016) A glassy carbon electrode modified with a nanocomposite consisting of MoS<sub>2</sub> and reduced graphene oxide for electrochemical simultaneous determination of ascorbic acid, dopamine, and uric acid. *Microchim Acta* 183:257–263
39. Rao D, Zhang X, Sheng Q, Zheng J (2016) Highly improved sensing of dopamine by using glassy carbon electrode modified with MnO<sub>2</sub>, graphene oxide, carbon nanotubes and gold nanoparticles. *Microchim Acta* 183:2597–2604
40. Mei LP, Feng JJ, Wu L, Chen JR, Shen L, Xie Y, Wang AJ (2016) A glassy carbon electrode modified with porous Cu<sub>2</sub>O nanospheres on reduced graphene oxide support for simultaneous sensing of uric acid and dopamine with high selectivity over ascorbic acid. *Microchim Acta* 183:2039–2046